

Published in final edited form as:

Neuron. 2014 June 18; 82(6): 1317–1333. doi:10.1016/j.neuron.2014.05.015.

Reduced cognition in *Syngap1* mutants is caused by isolated damage within developing forebrain excitatory neurons

Emin D. Ozkan^{1,*}, Thomas K. Creson^{1,*}, Enikő A. Kramár², Camilo Rojas¹, Ron R. Seese², Alex H. Babyan², Yulin Shi², Rocco Lucero³, Xiangmin Xu², Jeffrey L. Noebels³, Courtney A. Miller^{1,4}, Gary Lynch², and Gavin Rumbaugh^{1,#}

¹Department of Neuroscience, The Scripps Research Institute, Jupiter, FL, USA 33458

²Department of Anatomy and Neurobiology, The University of California, Irvine, CA, USA 92797

³Developmental Neurogenetics Laboratory, Departments of Neurology, Neuroscience and Molecular and Human Genetics, Baylor College of Medicine, Houston, TX, USA 77030

⁴Department of Metabolism and Aging, The Scripps Research Institute, Jupiter, FL, USA 33458

Summary

Syngap1 haploinsufficiency is a common cause of sporadic intellectual disability. *Syngap1* mutations disrupt developing pyramidal neurons, though it remains unclear if this process contributes to cognitive abnormalities. Here, we found that haploinsufficiency restricted to forebrain glutamatergic neurons was sufficient to disrupt cognition, while removing mutations from this population prevented cognitive abnormalities. In contrast, manipulating *Syngap1* function in GABAergic neurons had no effect on cognition, excitability or neurotransmission, highlighting the specificity of *Syngap1* mutations within forebrain excitatory neurons. Interestingly, cognitive abnormalities were reliably predicted by the emergence of enhanced excitatory synaptic function in mature superficial cortical pyramidal cells, which was a neurophysiological disruption caused by *Syngap1* dysfunction in developing, but not adult, forebrain neurons. We conclude that reduced cognition in *Syngap1* mutants is caused by isolated damage to developing forebrain glutamatergic neurons. This damage triggers secondary disruptions to synaptic homeostasis in mature cortical pyramidal cells, which perpetuates brain dysfunction into adulthood.

Introduction

Intellectual disability (ID) is characterized by low IQ and behavioral deficits, reaching a prevalence of 1–3% worldwide. This is a devastating brain disorder, where many patients are unable to care for themselves, placing a tremendous emotional and economic burden on

© 2014 Elsevier Inc. All rights reserved.

#Correspondence: Gavin Rumbaugh (grumbaugh@scripps.edu).

*EDO and TKC contributed equally to this work.

Publisher's Disclaimer: This is a PDF file of an unedited manuscript that has been accepted for publication. As a service to our customers we are providing this early version of the manuscript. The manuscript will undergo copyediting, typesetting, and review of the resulting proof before it is published in its final citable form. Please note that during the production process errors may be discovered which could affect the content, and all legal disclaimers that apply to the journal pertain.

families and society (Centers for Disease and Prevention, 2004; Doran et al., 2012). *SYNGAP1/Syngap1* (now referred to as *Syngap1* for simplicity) is among the most commonly mutated genes in sporadic ID. *De novo* autosomal dominant mutations in *Syngap1* that produce haploinsufficiency account for 2–8% of these cases, and the majority of patients have more severe forms of ID (Berryer et al., 2013; de Ligt et al., 2012; Hamdan et al., 2011a; Hamdan et al., 2011b; Hamdan et al., 2009; Krepischi et al., 2010; Rauch et al., 2012). Considering the relatively high prevalence of sporadic ID in the population, the surprising frequency of pathogenic *Syngap1* mutations in enriched patient populations suggest that there are tens-of-thousands of undocumented individuals carrying these mutations. Affected individuals also have a high incidence of childhood seizures and autism spectrum disorder (ASD). *Syngap1* haploinsufficiency has been causally linked to epileptic encephalopathy (EE), a devastating and often fatal form of childhood epilepsy that dramatically impairs cognitive development (Carvill et al., 2013). These recently identified EE patients with *Syngap1* mutations also share ID and ASD comorbidities. Thus, proper *Syngap1* gene dosage is essential for the normal development of human cognition and appears to modify important aspects of neural excitability and sociability.

The *Syngap1* Heterozygous knockout mouse line (*Syngap1*^{+/-}) has emerged as a robust model to understand the patho-neurobiology that underlies reduced cognitive ability and neural hyperexcitability in sporadic ID and epilepsy. *Syngap1*^{+/-} mice display significant cognitive, emotional, and social abnormalities, which support the idea that inactivating mutations of this gene directly cause cognitive impairment (Berryer et al., 2013; Guo et al., 2009; Komiyama et al., 2002; Muhia et al., 2010). Reduced *Syngap1* function in development accelerates the maturation of excitatory synaptic function in forebrain pyramidal cells (Clement et al., 2012; Clement et al., 2013), suggesting that damage to developing glutamatergic neurons may contribute to cognitive abnormalities in *Syngap1* mutants. However, a causal link between cognitive defects in *Syngap1* haploinsufficiency and developing glutamatergic neurons has not been shown. The change in glutamatergic neuron synapse development could be an inconsequential secondary outcome arising from dysfunction in other cell subtypes. Indeed, elegant studies in models of syndromic NDDs have shown that a single pathogenic mutation can affect the function of various cell types in the brain (Chao et al., 2010; Lioy et al., 2011). Furthermore, these studies demonstrate that multiple cell types are sufficient to drive cognitive, behavioral and/or electrophysiological abnormalities in the CNS of NDD models. Thus, it remains unclear if altered development of glutamatergic neurons contributes importantly to cognitive deficits in *Syngap1* mutants. In addition, it is not known if other neuronal subtypes are also sufficient to drive cognitive abnormalities in these mice.

Complete restoration of *Syngap1* protein expression (SynGAP) in adult mutants has no detectable benefit on behavior and cognition, demonstrating that *Syngap1* haploinsufficiency is a disorder of brain development (Clement et al., 2012). Interestingly, all currently reported baseline neurophysiological abnormalities observed in young glutamatergic neurons of *Syngap1*^{+/-} mice, such as enhanced excitatory synaptic transmission, are transiently expressed during development (Clement et al., 2013)(Clement et al., 2012). Thus, it also remains unclear how *Syngap1* mutations in development affect adult brain function. Indeed,

because the abnormal cognition persists throughout life, these findings suggest that there are undiscovered neurophysiological abnormalities in adult mice that arise from abnormal brain development and reflect abnormal cognition. To explore causal links between *Syngap1* dysfunction in developing glutamatergic neurons, stabilized changes to adult brain function, and altered cognitive ability, we combined cell-type specific and inducible conditional mouse lines with behavioral endophenotyping and electrophysiology. Using this approach, we found that germline *Syngap1* mutations induced a persistent form of stabilized cortical hyperexcitability that lasted into adulthood. Remarkably, this was caused exclusively by abnormal function of developing glutamatergic neurons located in the forebrain, as no phenotypic role for *Syngap1* in neurons that release GABA was apparent. Unexpectedly, abnormalities in developing glutamatergic neurons caused an emergent, secondary disruption to glutamatergic synaptic strength in adult neurons that reliably predicted the presence of reduced cognition. These data demonstrate that altered neurodevelopmental processes in a single sensitive cell type can perpetuate brain dysfunction into adulthood by altering E/I balance through a disruption of synaptic homeostasis.

Results

Cortical hyperexcitability and progressively worsening superficial pyramidal cell E/I balance in adult *Syngap1* mutants

We sought to investigate how altered brain development in *Syngap1*^{+/-} mice disrupts the function of the adult CNS. First, we performed EEG analysis paired with video monitoring to examine spontaneous cortical activity in mutants (Fig. 1A), which revealed frequent and widespread cortical discharges of high amplitude in mature *Syngap1*^{+/-} mice (>12 wks), but not in wild type (wt) littermates. These epileptiform discharges were intermittent, ranging in frequency from 1–681/hour (average 81/hr). However, they did not coincide with any abnormal motor events. Interestingly, cortical generalized seizures with myoclonic features have also been reported in patients with *Syngap1* loss of function mutations (Berryer et al., 2013) and with lower cognitive ability (Carville et al., 2013). We reasoned that cortical hyperexcitability might reflect a reduced seizure threshold in adult mutants. A flurothyl-induced activation paradigm (Clement et al., 2012) revealed a clear reduction in seizure threshold in two distinct *Syngap1* haploinsufficient mouse lines (Fig. 1B). To determine if network hyperexcitability in mutants was preserved in ex vivo preparations, we performed fast voltage dye (VSD) imaging in acute brain slices derived from adult *Syngap1* animals. Slices from adult *Syngap1*^{+/-} mice resulted in significantly larger signals throughout the cortex when compared to slices derived from wt littermates (Fig. 1C).

Because SynGAP is a potent regulator of glutamatergic synapse function (Clement et al., 2012; Clement et al., 2013; Rumbaugh et al., 2006), we hypothesized that elevated unitary synaptic strength in cortical pyramidal neurons contributes to slice hyperexcitability. To test this idea, we measured miniature excitatory postsynaptic currents (mEPSCs) from mPFC Layer 2/3 neurons in acute slices prepared from wt or *Syngap1*^{+/-} mice (Fig 2A,B). Interestingly, mEPSCs were normal in young cortical neurons (Fig. 2C–E). However, by adulthood, there was an increase in both the amplitude and frequency of the events (Fig. 2F–H). We also patched neurons in slices derived from the *Syngap1*^{+/*lx-st*} mice. Neurons from

this mouse line also exhibited enhanced mEPSC function in Layer 2/3 neurons (Fig. 2I–K). To determine if the E/I ratio was disrupted in Layer 2/3 pyramidal neurons, we acquired miniature inhibitory postsynaptic currents (mIPSCs) from neurons in slices derived from adult *Syngap1*^{+/-} or wt littermates. There was a reduction in mIPSC amplitude in conventional *Syngap1*^{+/-} mice (Fig. 2L), but no change in mIPSC properties in the *Syngap1*^{+/lx-st} mice (Fig. 2M). However, because excitatory unitary synaptic strength was increased in both models relative to GABAergic neuron synaptic transmission, this is consistent with an elevated E/I ratio in mature mPFC cortical neurons in mice with *Syngap1* haploinsufficiency. Furthermore, L2/3 neurons were hyperexcitable in response to evoked neurotransmitter release (Fig. S1). We next measured electrically isolated excitatory and inhibitory evoked responses from individual L2/3 pyramidal cells in mPFC slices from adult wt and *Syngap1* mutants (Fig. S1A–C). There was no significant effect of peak excitatory responses in the basal pathway; though there was an increase in the slope of the input/output curve (Fig. S1D–E). Importantly, evoked E/I balance was significantly shifted in both pathways (Fig. S1L–M), which is consistent with our mEPSC/mIPSC data and supports the conclusion that L2/3 neurons are hyperexcitable in *Syngap1* mutants.

To this point, our measurements have been restricted to synaptic properties of Layer 2/3 pyramidal neurons. However, there are other possible cellular causes of network hyperexcitability, such as alterations to the function of distinct classes of local inhibitory neurons in the superficial cortex (Fig 2B). Therefore, we probed *Syngap1* mutants for changes in two major subtypes of cortical GABAergic neurons. To label Parvalbumin-positive (PV+) neurons in the *Syngap1*^{+/-} background, we crossed *Syngap1*^{+/-} mice that also contained the Ai9 Cre-dependent reporter allele (Madisen et al., 2010) with PV+*-ires*-Cre driver mice (Hippenmeyer et al., 2005) (Fig. 3A). tdTomato+ (TD+) neurons from both genotypes exhibited properties consistent with PV+ neurons (Table S1) (Helm et al., 2013; Lazarus and Huang, 2011). There were no genotype differences in firing properties of these cells at PND 14 (Fig. 3B). In contrast, there was a substantial decrease in firing rate in PV+ neurons in *Syngap1*^{+/-} mice by six weeks of age (Fig. 3C), which was consistent with cortical hyperexcitability. Interestingly, by nine weeks of age, the difference between genotypes was no longer significant (Fig. 3D). We next measured unitary synaptic strength onto PV+ neurons in mature animals. Overall, there was a small reduction in mEPSC amplitude in PV+ neurons (Fig. 3E). However, this was only present in males (Two-way ANOVA for PV+ mEPSC amplitude: genotype effect, $F_{(1,61)}=6.00$, $p=0.02$; sex effect $F_{(1,61)}=5.01$, $p=0.03$; genotype*sex $F_{(1,61)}=4.72$, $p=0.03$). In contrast, there was no sex-genotype interaction in L2/3 pyramidal cell mEPSC properties (Two-way ANOVA for layer2/3 neuron mEPSC amplitude: genotype effect, $F_{(1,102)}=11.22$, $p=0.0011$; sex effect, $F_{(1,102)}=6.24$, $p=0.014$; genotype*sex, $F_{(1,102)}=0.054$, $p=0.81$. Two-way ANOVA for layer2/3 neuron mEPSC frequency: genotype effect, $F_{(1,102)}=17.42$, $p=6.29 \times 10^{-5}$; sex effect, $F_{(1,102)}=0.003$, $p=0.96$; genotype*sex, $F_{(1,102)}=0.35$, $p=0.55$; combined data). Thus, PV+ neurons may contribute to hyperexcitability at some stages of development, but individual changes in cellular and synaptic properties in these neurons do not stabilize in the fully mature CNS. We next probed for potential cellular disruptions in Somatostatin-positive (SST+) local inhibitory neurons. Surprisingly, there were no genotype effects in any major cellular or synaptic measures in adult (>9 wks) SST+ neurons (Fig 3F–I; Table S1). There

was a robust increase in action potential width of these neurons. However, this is a relatively minor physiological disruption with an unknown impact on network function (Table S1). Together, these data indicate that critical measures of inhibition are largely unaffected in the fully mature superficial cortex of *Syngap1* mutants.

E/I imbalance predicts cognitive abnormalities and results from *Syngap1* dysfunction exclusively in glutamatergic neurons of the developing, but not mature, forebrain

Increased pyramidal cell excitatory synaptic strength appeared to be a reliable signature of altered neurophysiological function in the mutant cortex, suggesting that *Syngap1* haploinsufficiency is principally a disease of altered glutamatergic neuron function. However, an abundance of SynGAP protein is found in both glutamatergic and GABAergic neurons in various cortical and subcortical areas of the brain, including heavy expression in the striatum (Moon et al., 2008; Porter et al., 2005; Zhang et al., 1999). Therefore, we explored the behavioral contribution of *in vivo Syngap1* dysfunction in distinct cellular populations. In the first set of experiments, we crossed the conditional knockout line (*Syngap1^{+fl}*) (Clement et al., 2012) with EMX1-ires-Cre driver mice (Gorski et al., 2002). This mouse driver line induces Cre-mediated recombination in forebrain glutamatergic neurons and glia (Fig. 4A). Importantly, SynGAP is a neuron-enriched gene (Chen et al., 1998; Kim et al., 1998; Kozlenkov et al., 2014) with no observable expression in glial cells (G. Rumbaugh, unpublished observation), indicating that this Cre driver line is an excellent tool to determine if *Syngap1* genetic damage in developing cortical pyramidal cells is sufficient to disrupt cognitive development. SynGAP levels were reduced in the hippocampus, but not striatum, in extracts taken from *Emx1-Cre;Syngap1^{+fl}* mice (Fig. 4B). Importantly, a reduction in SynGAP protein levels was also observed in the frontal cortex (Fig. S2). The behaviors displayed by *Emx1-Cre;Syngap1^{+fl}* mice were indistinguishable from conventional *Syngap1* mutants. Relative to wt littermates, *EMX1-Cre;Syngap1^{+fl}* mice spent more time in the open arm of the elevated plus maze (Fig. 4C), were hyperactive in the open field (Fig. 4D), and failed to spontaneously alternate (Fig. 4E). Conventional *Syngap1* Het mice had deficits in remote (30 day old) fear memory (Fig. S3), allowing us to include an additional measure of cognition in the behavioral battery. Again, similar to conventional *Syngap1* mutants, *Emx1-Cre;Syngap1^{+fl}* mice exhibited a remote memory deficit (Fig. 4F). We next assessed adult seizure threshold. Consistent with the behavioral endophenotyping results, the *Emx1-Cre;Syngap1^{+fl}* mice also had a reduced seizure threshold (Fig. 4G) that was qualitatively similar to conventional germline *Syngap1* mutants (Fig. 1B).

To induce haploinsufficiency in developing GABAergic neurons, we next crossed *Syngap1* conditional KO mice to *Gad2-ires-Cre* driver mice (Taniguchi et al., 2011) (Fig. 4H). A reduction in SynGAP expression in the striatum, but not hippocampus, confirmed haploinsufficiency in the target neuronal population (Fig. 4I). Unexpectedly, SynGAP levels in the hippocampus of *Gad2-Cre* mice increased slightly. Therefore, we also probed SynGAP expression levels in the frontal cortex of *Gad2-Cre;Syngap1^{+fl}* mice. There was no change in SynGAP expression (Fig. S2), which is consistent with low expression of SynGAP in cortical GABAergic neurons (Zhang et al., 1999). Surprisingly, despite SynGAP expression being reduced in GABAergic neurons in the CNS, including the striatum, there were no changes in behavior or seizure threshold (Fig. 4J-N).

If disruptions to forebrain glutamatergic neurons are the primary driver of the endophenotype in *Syngap1*^{+/-} mice, then rescuing the mutation exclusively in this population should protect animals from developing behavioral abnormalities. To test this, we crossed EMX1- or GAD2-ires-Cre driver mice to the *Syngap1* conditional rescue line (*Syngap1*^{+/*lx-st*}) (Clement et al., 2012) (Figure 5A,G). Remarkably, reversing the pathogenic mutations only in forebrain glutamatergic neurons (*Emx1-Cre;Syngap1*^{+/*lx-st*} mice) was sufficient to protect animals from developing major behavioral impairments, including altered anxiety and risk-taking, reduced working memory and disrupted remote contextual memory (Fig 5B–F). Interestingly, *Emx1-Cre;Syngap1*^{+/*lx-st*} mice were still hyperactive in the open field (Fig 5C) and exhibited a reduced seizure threshold (Fig 5F), suggesting that extra-cortical neurons contribute to these abnormalities. This notion was supported by the observation that seizure threshold was rescued after global reversal of *Syngap1* haploinsufficiency (Fig. S4). In a complementary set of experiments, reversal of a pathogenic *Syngap1* mutation in GABAergic neurons located throughout the entire CNS (*Gad2-Cre;Syngap1*^{+/*lx-st*}) provided no improvement to core *Syngap1* behavioral abnormalities (Fig 5H–L).

Enhanced excitatory synaptic function in mature pyramidal neurons is present in both of our models of *Syngap1* haploinsufficiency (Fig. 2F–K). These data suggested that this neurophysiological abnormality is predictive of cognitive dysfunction and/or hyperexcitability in *Syngap1* mutants. To test this, we patch-clamped layer 2/3 neurons in mPFC acute slices taken from EMX1- and *Gad2-ires-Cre* mice crossed to each of our conditional *Syngap1* mutant lines. Both *Emx1-Cre;Syngap1*^{+/*fl*} (forebrain glutamatergic conditional disruption) and *Gad2-Cre;Syngap1*^{+/*lx-st*} (GABAergic neuron rescue) animals, which were offspring that had reduced cognition and altered seizure thresholds (Fig. 4C–G; Fig. 5G–L), had enhanced excitatory synaptic strength in Layer 2/3 mPFC pyramidal neurons (Fig. 6A–C,J–K). Interestingly, no changes to pyramidal cell synaptic function were observed in either *Gad2-Cre;Syngap1*^{+/*fl*} (GABAergic conditional disruption) or *Emx1-Cre;Syngap1*^{+/*lx-st*} (forebrain glutamatergic neuron rescue) lines (Fig. 6D–I), which were offspring that had normal cognitive ability but altered seizure threshold. We also tested the reliability of the reduced mIPSCs observed in *Syngap1*^{+/-} line as a signature of cognitive ability, but found that neither *Emx1-Cre;Syngap1*^{+/*fl*} nor *Gad2-Cre;Syngap1*^{+/*fl*} displayed reduced mIPSCs (Fig. S5). These data indicate that excitatory synaptic function in mature superficial pyramidal neurons reliably predicts cognitive ability, but not behavioral seizure threshold, in adult *Syngap1* mutant mice.

In the next set of experiments, we further explored the relationship between enhanced excitatory synaptic strength in L2/3 pyramidal neurons and cognitive disability in *Syngap1* mutants. To do this, we induced global *Syngap1* haploinsufficiency in mature animals and then probed for physiological and behavioral changes (Fig. 7A). We first confirmed that tamoxifen injections reduced SynGAP protein by 50% in the experimental animals (Fig. 7B), which is the level of expression observed in germline heterozygous knockout mice (Clement et al., 2012). Despite the conditional reduction of SynGAP protein in adulthood, mEPSC amplitude or frequency were not changed (Fig. 7C,D), consistent with the idea that changes in adult Layer 2/3 pyramidal neuron excitatory synaptic function is a secondary

consequence of abnormal brain development. Based on our prior experiments demonstrating the predictive value of this adult physiological measure on cognitive ability, these data suggested that adult-induced haploinsufficiency would have negligible effects on cognition. Indeed, there was no change in core *Syngap1* behaviors; open field locomotion (Fig. 7E), elevated plus maze open arm time (Fig. 7F), the ability to spontaneously alternate in a T-maze (Fig. 7G) and remote memory (Fig. 7H). However, seizure threshold was reduced (Fig. 7I,J), indicating that this behavior is dissociable from cognitive dysfunction and elevated cortical pyramidal cell excitatory synaptic function in *Syngap1* mutants.

We next wanted to further explore the idea that stronger excitatory synaptic function in L2/3 pyramidal cells was unrelated to reduced SynGAP function in mature neurons, but instead is caused by a complex molecular process that originates within developing superficial pyramidal neurons. To test this, we exploited the ability to reverse pathogenic *Syngap1* mutations globally in the CNS (Clement et al., 2012). As a proof of principle, however, we first sought to discover a neurophysiological disruption in adult *Syngap1* mice that was sensitive to adult genetic reversal in order to demonstrate the effectiveness of this mouse model as tool to differentiate developmental versus homeostatic consequences of pathogenic *Syngap1* mutations in brain cells. We chose to focus on LTP deficits because they are well described in *Syngap1* Hets (Kim et al., 2003; Komiyama et al., 2002). Axonal excitability, release, and postsynaptic responses were not affected by *Syngap1* haploinsufficiency (Fig. 8A–C), though stabilization of LTP was drastically impaired in adult mutants (Fig. 8D). Strikingly, LTP deficits were completely rescued by adult reversal of the pathogenic mutation (Fig. 8D). We next conducted Fluorescence Deconvolution Tomography (Chen et al., 2007; Vogel-Ciernia et al., 2013) to gain molecular insight into how pathogenic *Syngap1* mutations could disrupt the synaptic signaling steps thought to be involved in LTP consolidation (Rex et al., 2009). Slices were collected two minutes after LTP-inducing theta bursts and immunostained for PSD95 and Ras-GTP or phosphorylated ERK1/2 (Fig. 8E). Theta bursts doubled the number of Ras-GTP+ excitatory synapses associated with high levels of Ras-GTP ($p=0.012$, t-test, 2-tails) in wt, but not mutants ($p>0.10$) (Fig. 8F, *left panel*). A similar pattern was found for p-ERK1/2; theta stimulation caused a pronounced increase in the double-labeled contacts in wt slices ($p<0.0001$), but had no detectable effect in Hets ($p>0.95$). Note that baseline levels of PSDs associated with high concentrations of p-ERK were substantially and significantly elevated relative to wild-types in the mutants ($p=0.029$, U-Test) (*right panel*; Fig. 8F), indicating that reduced SynGAP protein in mature spines derepresses resting levels of activated ERK1/2. In accordance with the LTP results, conditional rescue of *Syngap1* haploinsufficiency returned the pERK1/2 response to theta bursts to levels obtained in wt mice (control vs. theta bursts: $p=0.002$). We further investigated group differences by counting the number of double-labeled synapses at various intensities of pERK1/2 immunostaining, an analysis that included all pERK positive contacts. Theta bursts shifted the frequency distribution to the right in wt mice ($p<0.0001$, two-way ANOVA) (Fig. 8G), as expected if the LTP-inducing stimulation increased the pool of activated kinase at a relatively small subset of synapses. A similar effect was observed for slices prepared from conditional rescue mice ($p<0.0001$; Figure 8H), but was altogether absent ($p>0.95$) in Hets (Fig. 8I).

Finally, we measured mEPSCs from mPFC L2/3 pyramidal cells in wt, Het and rescue animals to examine how SynGAP expression levels in adulthood influence this neurophysiological disruption that is also present in adult *Syngap1* mutants. In striking contrast to the hippocampal plasticity deficits, elevated synaptic strength in L2/3 Het pyramidal neurons was not improved by the adult genetic repair strategy (Fig 8J–K). Importantly, we confirmed that the frontal cortex of conventional *Syngap1* Hets also have elevated levels of p-ERK1/2 (Fig. S6). Together, these findings support the idea that enhanced excitatory synaptic strength in superficial cortical pyramidal cells arises from developmental neuronal damage, while also indicating that this neurophysiological disruption is independent of homeostatic alterations to Ras/ERK dendritic spine signaling caused by low SynGAP levels in adult neurons. These data also further validate the predictive value of enhanced L2/3 excitatory synaptic strength in Het mice because adult reversal of pathogenic *Syngap1* mutations does not improve performance in behavioral measures of cognition (Clement et al., 2012).

Discussion

There is a great interest in defining the brain regions and specific cell types responsible for cognitive deficits in NDDs, with the hope of developing tailor-made therapies for each specific condition. Prior studies in other models of NDDs suggest that cognition and behavioral adaptations are impaired through defects in a wide variety of cell types and circuits. However, not all cell types expressing the mutation are required to reproduce important elements of the disorder. For example, deletion of *MECP2* in GABAergic neurons phenotypically mimics the constitutive germline deletion (Chao et al., 2010), while restoration of gene function in glia provides significant rescue (Lioy et al., 2011). A similar relationship between GABAergic neuron dysfunction and *NF1* mutations also exists (Cui et al., 2008). Interestingly, *NF1*, like *Syngap1*, is a RasGAP, though there is a clear distinction between the cell and temporal-specificity mediated by disruption to these two ID-related genes (*please see supplemental discussion for a detailed comparison of these two RasGAP-related ID models*). Cell type and brain region specificity has also been extensively studied in the *Tsc1* model, where cerebellar neurons, astrocytes, and thalamic excitatory neurons have been implicated in various behavioral phenotypes (Meikle et al., 2007; Normand et al., 2013; Tsai et al., 2012; Uhlmann et al., 2002). Although cortical hyperexcitability has been shown to result from excitatory neurons in *Fmr1* KO mice, cell type specificity of cognitive defects have not been thoroughly examined (Hays et al., 2011). Due to the robust nature of cognitive deficits in *Syngap1*^{+/-} mice, we succeeded in identifying a sensitive cell type (e.g. forebrain pyramidal neurons) that is both necessary and sufficient to account for the bulk of the behavioral endophenotype. This specificity is highlighted by the minimal functional impact of these mutations in other cell types, such as GABAergic neurons located throughout the CNS. In addition to all forebrain pyramidal neurons, the *EMX1* driver line used in this study causes Cre-mediated recombination in glial and Cajal-Retzius cells (Gorski et al., 2002). *Syngap1* is highly enriched in neurons (Kim et al., 1998). Thus, glia are unlikely to underlie major aspects of the mouse endophenotype. However, our results cannot rule out the possibility that other cell types, such as Cajal-Retzius cells, contribute to cognitive defects in *Syngap1* Hets.

Enhanced excitatory synaptic drive onto mature superficial pyramidal neurons resulting from the developmental impact of pathogenic *Syngap1* mutations may disrupt the computational power of local synaptic networks by impacting the coding of information (Petersen and Crochet, 2013). This idea is supported by the current findings of abnormal cortical discharges in mature *Syngap1* mutants. Interestingly, similar cortical discharges are observed in human *Syngap1* haploinsufficiency patients (Berryer et al., 2013) and the presence of these types of high-frequency oscillations in humans is associated with reduced cognition (Nicolai et al., 2012). As a result, even if cellular and/or network signatures of hyperexcitability cannot be directly linked to reduced cognition in mature *Syngap1*^{+/-} mice, the presence of similar measures of abnormal EEG signals in both mice and humans with pathogenic *Syngap1* mutations indicates the potential for them to serve as a robust endpoint in translational studies aimed at improving brain function and cognitive ability in patients.

Our current studies employing temporal and cell type-specific alterations of SynGAP expression further support the emerging idea that pathogenic *Syngap1* mutations cause cognitive abnormalities through developmental brain damage (Clement et al., 2012; Clement et al., 2013). Although we do not know the exact role of *Syngap1* during the developmental critical period, one possibility is that early synapse maturation caused by pathogenic disruptions to this gene (Clement et al., 2012; Clement et al., 2013) may permanently fix the adult spines to a larger size. Indeed, we have found that newly born spines in the developing *Syngap1* mutant brain are larger than nascent spines born to wt neurons (M. Aceti and G. Rumbaugh, unpublished observations). Dendritic spine volume is tightly coupled to AMPA receptor function at individual postsynapses in both the cortex and hippocampus (Matsuzaki et al., 2001; Noguchi et al., 2011). Thus, abnormally large spines in mature cortical pyramidal cells in *Syngap1* mice may degrade the ability of these neurons to scale down synaptic excitation in response to environmental stimuli or changing social conditions (Wang et al., 2011). Indeed, according to the principle of homeostatic regulation of neuronal firing rates (Turrigiano, 2008), excitatory synapses in *Syngap1* mutants would be expected to scale down their strengths to compensate for the enhanced network excitability that is clearly present in these mice. Thus, the gradual emergence of elevated excitatory synaptic function in Layer 2/3 neurons as a secondary consequence of *Syngap1* disruption in development is representative of an altered form of synaptic homeostasis that degrades the ability of mature Layer 2/3 neurons to optimally balance excitation relative to inhibition.

Experimental Procedures (Brief)

The generation of conventional *Syngap1*^{+/-} mice (Kim et al., 2003), conditional knockout line (*Syngap1*^{+/fl}) and conditional rescue line (*Syngap1*^{+/lx-st}) has been described previously (Clement et al., 2012). All *Syngap1* mice are maintained on a BL6/B129sv/ev hybrid background as previously described (Clement et al., 2012; Guo et al., 2009). *Emx1*-Cre (#05628), *Gad2*-Cre (#10802), *PV*-Cre (#8069), Inducible CAG-Cre-ERT (#004682), *TdTomato Ai9* (#007905) and *GIN-GFP* (#03718) lines were purchased from Jackson Laboratories. According to the supplier, these lines are maintained on a pure C57/BL6j background (N>5 generations), except for the *PV*-Cre line, which is on a hybrid B6;129p2 background, and the *GIN-GFP* line, which is on a FVB/NJ background. In general, male Cre drivers were used in mating schemes, except for *EMX1*-ires-Cre crosses, due to rare

occurrences of Cre activity in sperm cells. Video EEG recordings lasted for two weeks and random samples of the recordings were analyzed for evidence of spiking. VSD imaging in cortical slices was performed as previously described (Clement et al., 2012; Xu et al., 2010). mPFC slices for whole cell electrophysiology experiments were prepared as described elsewhere (Clement et al., 2013). Behavioral paradigms, tamoxifen injections and fluoroethyl-induced seizure protocol were carried out as described previously (Clement et al., 2012). Extracellular slice physiology and Fluorescence Deconvolution Tomography has been described in detail elsewhere (Babayan et al., 2012; Chen et al., 2010; Chen et al., 2007; Vogel-Ciernia et al., 2013). For precise details pertaining to all experimental procedures used in this in this study, please refer to the supplemental methods section of the manuscript.

Supplementary Material

Refer to Web version on PubMed Central for supplementary material.

Acknowledgments

GR was supported by The National Institute for Neurological Disorders and Stroke (R01NS064079) and The National Institute for Mental Health (R01MH096847). CAM was supported by grants from the National Institute for Drug Abuse (R01 DA034116; R03 DA033499). GR and CAM were both supported by the Scripps Florida Fund. JLN was supported by The National Institute for Neurological Disorders and Stroke grant NS29709. GL was supported by The National Institute for Neurological Disorders and Stroke grants NS085709 and NS045260 and the UCI Center for Autism Research and Treatment.

References

- Babayan AH, Kramar EA, Barrett RM, Jafari M, Haettig J, Chen LY, Rex CS, Lauterborn JC, Wood MA, Gall CM, Lynch G. Integrin dynamics produce a delayed stage of long-term potentiation and memory consolidation. *The Journal of neuroscience: the official journal of the Society for Neuroscience*. 2012; 32:12854–12861. [PubMed: 22973009]
- Berryer MH, Hamdan FF, Klitten LL, Moller RS, Carmant L, Schwartzenruber J, Patry L, Dobrzyniecka S, Rochefort D, Neugnot-Cerioli M, et al. Mutations in SYNGAP1 cause intellectual disability, autism, and a specific form of epilepsy by inducing haploinsufficiency. *Human mutation*. 2013; 34:385–394. [PubMed: 23161826]
- Carvill GL, Heavin SB, Yendle SC, McMahon JM, O’Roak BJ, Cook J, Khan A, Dorschner MO, Weaver M, Calvert S, et al. Targeted resequencing in epileptic encephalopathies identifies de novo mutations in CHD2 and SYNGAP1. *Nature genetics*. 2013; 45:825–830. [PubMed: 23708187]
- Centers for Disease C and Prevention . Economic costs associated with mental retardation, cerebral palsy, hearing loss, and vision impairment--United States, 2003. *MMWR Morbidity and mortality weekly report*. 2004; 53:57–59. [PubMed: 14749614]
- Chao HT, Chen H, Samaco RC, Xue M, Chahrour M, Yoo J, Neul JL, Gong S, Lu HC, Heintz N, et al. Dysfunction in GABA signalling mediates autism-like stereotypies and Rett syndrome phenotypes. *Nature*. 2010; 468:263–269. [PubMed: 21068835]
- Chen HJ, Rojas-Soto M, Oguni A, Kennedy MB. A synaptic Ras-GTPase activating protein (p135 SynGAP) inhibited by CaM kinase II. *Neuron*. 1998; 20:895–904. [PubMed: 9620694]
- Chen LY, Rex CS, Babayan AH, Kramar EA, Lynch G, Gall CM, Lauterborn JC. Physiological activation of synaptic Rac>PAK (p-21 activated kinase) signaling is defective in a mouse model of fragile X syndrome. *The Journal of neuroscience: the official journal of the Society for Neuroscience*. 2010; 30:10977–10984. [PubMed: 20720104]
- Chen LY, Rex CS, Casale MS, Gall CM, Lynch G. Changes in synaptic morphology accompany actin signaling during LTP. *The Journal of neuroscience: the official journal of the Society for Neuroscience*. 2007; 27:5363–5372. [PubMed: 17507558]

- Clement JP, Aceti M, Creson TK, Ozkan ED, Shi Y, Reish NJ, Almonte AG, Miller BH, Wiltgen BJ, Miller CA, et al. Pathogenic SYNGAP1 mutations impair cognitive development by disrupting maturation of dendritic spine synapses. *Cell*. 2012; 151:709–723. [PubMed: 23141534]
- Clement JP, Ozkan ED, Aceti M, Miller CA, Rumbaugh G. SYNGAP1 Links the Maturation Rate of Excitatory Synapses to the Duration of Critical-Period Synaptic Plasticity. *The Journal of neuroscience: the official journal of the Society for Neuroscience*. 2013; 33:10447–10452. [PubMed: 23785156]
- Cui Y, Costa RM, Murphy GG, Elgersma Y, Zhu Y, Gutmann DH, Parada LF, Mody I, Silva AJ. Neurofibromin regulation of ERK signaling modulates GABA release and learning. *Cell*. 2008; 135:549–560. [PubMed: 18984165]
- de Ligt J, Willemsen MH, van Bon BW, Kleefstra T, Yntema HG, Kroes T, Vulto-van Silfhout AT, Koolen DA, de Vries P, Gilissen C, et al. Diagnostic exome sequencing in persons with severe intellectual disability. *The New England journal of medicine*. 2012; 367:1921–1929. [PubMed: 23033978]
- Doran CM, Einfeld SL, Madden RH, Otim M, Horstead SK, Ellis LA, Emerson E. How much does intellectual disability really cost? First estimates for Australia. *Journal of intellectual & developmental disability*. 2012; 37:42–49. [PubMed: 22339044]
- Gorski JA, Talley T, Qiu M, Puelles L, Rubenstein JL, Jones KR. Cortical excitatory neurons and glia, but not GABAergic neurons, are produced in the Emx1-expressing lineage. *The Journal of neuroscience: the official journal of the Society for Neuroscience*. 2002; 22:6309–6314. [PubMed: 12151506]
- Guo X, Hamilton PJ, Reish NJ, Sweatt JD, Miller CA, Rumbaugh G. Reduced expression of the NMDA receptor-interacting protein SynGAP causes behavioral abnormalities that model symptoms of Schizophrenia. *Neuropsychopharmacology: official publication of the American College of Neuropsychopharmacology*. 2009; 34:1659–1672. [PubMed: 19145222]
- Hamdan FF, Daoud H, Piton A, Gauthier J, Dobrzeniecka S, Krebs MO, Joober R, Lacaille JC, Nadeau A, Milunsky JM, et al. De novo SYNGAP1 mutations in nonsyndromic intellectual disability and autism. *Biological psychiatry*. 2011a; 69:898–901. [PubMed: 21237447]
- Hamdan FF, Gauthier J, Araki Y, Lin DT, Yoshizawa Y, Higashi K, Park AR, Spiegelman D, Dobrzeniecka S, Piton A, et al. Excess of de novo deleterious mutations in genes associated with glutamatergic systems in nonsyndromic intellectual disability. *American journal of human genetics*. 2011b; 88:306–316. [PubMed: 21376300]
- Hamdan FF, Gauthier J, Spiegelman D, Noreau A, Yang Y, Pellerin S, Dobrzeniecka S, Cote M, Perreau-Linck E, Carmant L, et al. Mutations in SYNGAP1 in autosomal nonsyndromic mental retardation. *The New England journal of medicine*. 2009; 360:599–605. [PubMed: 19196676]
- Hays SA, Huber KM, Gibson JR. Altered neocortical rhythmic activity states in Fmr1 KO mice are due to enhanced mGluR5 signaling and involve changes in excitatory circuitry. *The Journal of neuroscience: the official journal of the Society for Neuroscience*. 2011; 31:14223–14234. [PubMed: 21976507]
- Helm J, Akgul G, Wollmuth LP. Subgroups of parvalbumin-expressing interneurons in layers 2/3 of the visual cortex. *Journal of neurophysiology*. 2013; 109:1600–1613. [PubMed: 23274311]
- Hippenmeyer S, Vrieseling E, Sigrist M, Portmann T, Laengle C, Ladle DR, Arber S. A developmental switch in the response of DRG neurons to ETS transcription factor signaling. *PLoS biology*. 2005; 3:e159. [PubMed: 15836427]
- Kim JH, Lee HK, Takamiya K, Haganir RL. The role of synaptic GTPase-activating protein in neuronal development and synaptic plasticity. *The Journal of neuroscience: the official journal of the Society for Neuroscience*. 2003; 23:1119–1124. [PubMed: 12598599]
- Kim JH, Liao D, Lau LF, Haganir RL. SynGAP: a synaptic RasGAP that associates with the PSD-95/SAP90 protein family. *Neuron*. 1998; 20:683–691. [PubMed: 9581761]
- Komiyama NH, Watabe AM, Carlisle HJ, Porter K, Charlesworth P, Monti J, Strathdee DJ, O'Carroll CM, Martin SJ, Morris RG, et al. SynGAP regulates ERK/MAPK signaling, synaptic plasticity, and learning in the complex with postsynaptic density 95 and NMDA receptor. *The Journal of neuroscience: the official journal of the Society for Neuroscience*. 2002; 22:9721–9732. [PubMed: 12427827]

- Kozlenkov A, Roussos P, Timashpolsky A, Barbu M, Rudchenko S, Bibikova M, Klotzle B, Byne W, Lyddon R, Di Narzo AF, et al. Differences in DNA methylation between human neuronal and glial cells are concentrated in enhancers and non-CpG sites. *Nucleic acids research*. 2014; 42:109–127. [PubMed: 24057217]
- Krepischi AC, Rosenberg C, Costa SS, Crolla JA, Huang S, Vianna-Morgante AM. A novel de novo microdeletion spanning the SYNGAP1 gene on the short arm of chromosome 6 associated with mental retardation. *American journal of medical genetics Part A*. 2010; 152A:2376–2378. [PubMed: 20683986]
- Lazarus MS, Huang ZJ. Distinct maturation profiles of perisomatic and dendritic targeting GABAergic interneurons in the mouse primary visual cortex during the critical period of ocular dominance plasticity. *Journal of neurophysiology*. 2011; 106:775–787. [PubMed: 21613595]
- Lioy DT, Garg SK, Monaghan CE, Raber J, Foust KD, Kaspar BK, Hirrlinger PG, Kirchhoff F, Bissonnette JM, Ballas N, Mandel G. A role for glia in the progression of Rett's syndrome. *Nature*. 2011; 475:497–500. [PubMed: 21716289]
- Madisen L, Zwingman TA, Sunkin SM, Oh SW, Zariwala HA, Gu H, Ng LL, Palmiter RD, Hawrylycz MJ, Jones AR, et al. A robust and high-throughput Cre reporting and characterization system for the whole mouse brain. *Nature neuroscience*. 2010; 13:133–140.
- Matsuzaki M, Ellis-Davies GC, Nemoto T, Miyashita Y, Iino M, Kasai H. Dendritic spine geometry is critical for AMPA receptor expression in hippocampal CA1 pyramidal neurons. *Nature neuroscience*. 2001; 4:1086–1092.
- Meikle L, Talos DM, Onda H, Pollizzi K, Rotenberg A, Sahin M, Jensen FE, Kwiatkowski DJ. A mouse model of tuberous sclerosis: neuronal loss of Tsc1 causes dysplastic and ectopic neurons, reduced myelination, seizure activity, and limited survival. *The Journal of neuroscience: the official journal of the Society for Neuroscience*. 2007; 27:5546–5558. [PubMed: 17522300]
- Moon IS, Sakagami H, Nakayama J, Suzuki T. Differential distribution of synGAP alpha1 and synGAP beta isoforms in rat neurons. *Brain research*. 2008; 1241:62–75. [PubMed: 18824155]
- Muhia M, Yee BK, Feldon J, Markopoulos F, Knuesel I. Disruption of hippocampus-regulated behavioural and cognitive processes by heterozygous constitutive deletion of SynGAP. *The European journal of neuroscience*. 2010; 31:529–543. [PubMed: 20105235]
- Nicolai J, Ebus S, Biemans DP, Arends J, Hendriksen J, Vles JS, Aldenkamp AP. The cognitive effects of interictal epileptiform EEG discharges and short nonconvulsive epileptic seizures. *Epilepsia*. 2012; 53:1051–1059. [PubMed: 22554146]
- Noguchi J, Nagaoka A, Watanabe S, Ellis-Davies GC, Kitamura K, Kano M, Matsuzaki M, Kasai H. In vivo two-photon uncaging of glutamate revealing the structure-function relationships of dendritic spines in the neocortex of adult mice. *The Journal of physiology*. 2011; 589:2447–2457. [PubMed: 21486811]
- Normand EA, Crandall SR, Thorn CA, Murphy EM, Voelcker B, Browning C, Machan JT, Moore CI, Connors BW, Zervas M. Temporal and Mosaic Tsc1 Deletion in the Developing Thalamus Disrupts Thalamocortical Circuitry, Neural Function, and Behavior. *Neuron*. 2013
- Petersen CC, Crochet S. Synaptic computation and sensory processing in neocortical layer 2/3. *Neuron*. 2013; 78:28–48. [PubMed: 23583106]
- Porter K, Komiyama NH, Vitalis T, Kind PC, Grant SG. Differential expression of two NMDA receptor interacting proteins, PSD-95 and SynGAP during mouse development. *The European journal of neuroscience*. 2005; 21:351–362. [PubMed: 15673435]
- Rauch A, Wiczorek D, Graf E, Wieland T, Ende S, Schwarzmayr T, Albrecht B, Bartholdi D, Beygo J, Di Donato N, et al. Range of genetic mutations associated with severe non-syndromic sporadic intellectual disability: an exome sequencing study. *The Lancet*. 2012; 380:1674–1682.
- Rex CS, Chen LY, Sharma A, Liu J, Babayan AH, Gall CM, Lynch G. Different Rho GTPase-dependent signaling pathways initiate sequential steps in the consolidation of long-term potentiation. *The Journal of cell biology*. 2009; 186:85–97. [PubMed: 19596849]
- Rumbaugh G, Adams JP, Kim JH, Haganir RL. SynGAP regulates synaptic strength and mitogen-activated protein kinases in cultured neurons. *Proceedings of the National Academy of Sciences of the United States of America*. 2006; 103:4344–4351. [PubMed: 16537406]

- Taniguchi H, He M, Wu P, Kim S, Paik R, Sugino K, Kvitsiani D, Fu Y, Lu J, Lin Y, et al. A resource of Cre driver lines for genetic targeting of GABAergic neurons in cerebral cortex. *Neuron*. 2011; 71:995–1013. [PubMed: 21943598]
- Tsai PT, Hull C, Chu Y, Greene-Colozzi E, Sadowski AR, Leech JM, Steinberg J, Crawley JN, Regehr WG, Sahin M. Autistic-like behaviour and cerebellar dysfunction in Purkinje cell Tsc1 mutant mice. *Nature*. 2012; 488:647–651. [PubMed: 22763451]
- Turrigiano GG. The self-tuning neuron: synaptic scaling of excitatory synapses. *Cell*. 2008; 135:422–435. [PubMed: 18984155]
- Uhlmann EJ, Wong M, Baldwin RL, Bajenaru ML, Onda H, Kwiatkowski DJ, Yamada K, Gutmann DH. Astrocyte-specific TSC1 conditional knockout mice exhibit abnormal neuronal organization and seizures. *Annals of neurology*. 2002; 52:285–296. [PubMed: 12205640]
- Vogel-Ciernia A, Matheos DP, Barrett RM, Kramar EA, Azzawi S, Chen Y, Magnan CN, Zeller M, Sylvain A, Haettig J, et al. The neuron-specific chromatin regulatory subunit BAF53b is necessary for synaptic plasticity and memory. *Nature neuroscience*. 2013; 16:552–561.
- Wang F, Zhu J, Zhu H, Zhang Q, Lin Z, Hu H. Bidirectional control of social hierarchy by synaptic efficacy in medial prefrontal cortex. *Science*. 2011; 334:693–697. [PubMed: 21960531]
- Xu X, Olivas ND, Levi R, Ikrar T, Nenadic Z. High precision and fast functional mapping of cortical circuitry through a novel combination of voltage sensitive dye imaging and laser scanning photostimulation. *Journal of neurophysiology*. 2010; 103:2301–2312. [PubMed: 20130040]
- Zhang W, Vazquez L, Apperson M, Kennedy MB. Citron binds to PSD-95 at glutamatergic synapses on inhibitory neurons in the hippocampus. *The Journal of neuroscience: the official journal of the Society for Neuroscience*. 1999; 19:96–108. [PubMed: 9870942]

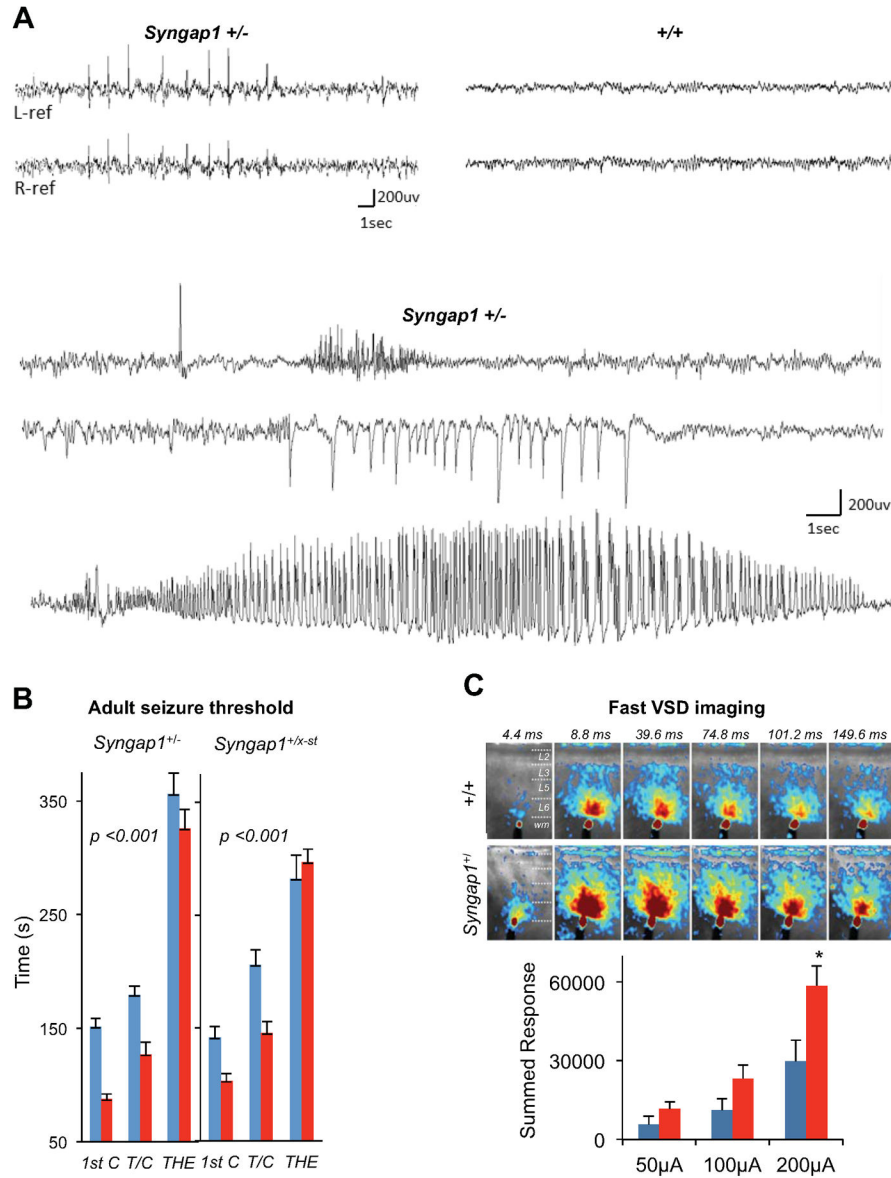


Figure 1. Altered EEG activity, reduced seizure threshold and cortical hyperexcitability in adult *Syngap1*^{+/-} mice

(A) Representative cortical EEG traces from chronically implanted, behaving *Syngap1*^{+/-} conventional mutant mice (n=3) reveal frequent generalized sharp epileptiform discharges (upper left), and occasional brief (<1 s) or prolonged (>10 s) seizures with a myoclonic jerk or little behavioral accompaniment during video monitoring (lower three traces). Wild type mice (n=2) showed no evidence of hyperactive EEG spike discharges or seizures (top right). Electrodes record bilaterally from temporal and parietal cortices over left and right hemispheres in upper traces, and from left parietal cortex in lower seizure traces.

(B) Reduced flurothyl seizure threshold in both *Syngap1*^{+/-} and *Syngap1*^{+/-}/*x-st* mutant mice (red bars) compared to wild-type controls (blue bars). Time (in seconds) taken to reach three separate events, first clonus (1st C), tonic-clonic (T/C), and total hindlimb extension

(THE), during the course of the procedure were measured and plotted in the y axis. *Syngap1*^{+/-}: RMANOVA; genotype effect, $F(1,19)=20.46$, $p=0.00023$; genotype x event interaction, $F(2, 38)=0.99$, $p=0.38$. *Syngap1*^{+/-x-st}: RMANOVA; genotype effect, $F(1,24)=5.47$, $p=0.028$; genotype x event interaction, $F(2,48)=6.46$, $p=0.0033$.

(C) *Syngap1*^{+/-} mPFC slices exhibit higher evoked excitability compared to wild type control slices, when examined with fast voltage sensitive dye (VSD) imaging. (Top) Example time series data from VSD imaging of evoked circuit activity in response to electrical stimulation of 200 μA at 1ms. All image frames were averaged over eight separate trials. The color scale codes VSD signal amplitude expressed as SD (standard deviation) multiples above the mean baseline. Warmer colors indicate greater excitation. (Bottom) Pixel-based response analysis (see methods). The y-axis shows the summed response (in the SD multiple units) across the defined response frames to electrical stimulation. Student's t test: 50 μA , $n=7$ wt, $n=7$ mutant, $t(12)=1.44$, $p=0.18$; 100 μA , $n=8$ wt, $n=8$ mutant, $t(14)=1.78$, $p=0.096$; 200 μA , $n=8$ wt, $n=7$ mutant, $t(13)=2.59$, $p=0.022$. Wild-type(+/+), blue; mutants(+/-), red for all bar graphs. Error bars denote +SEM. * $p<0.05$.

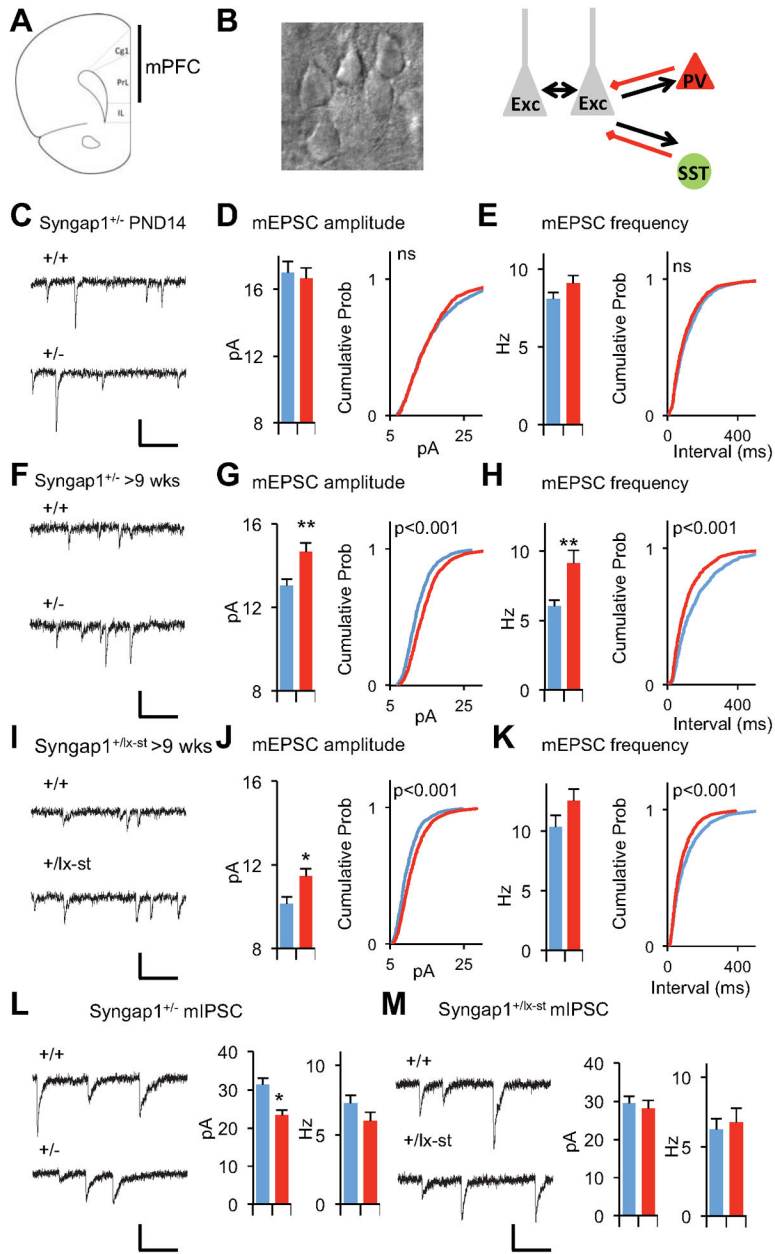


Figure 2. The gradual development of E/I imbalance in layer 2/3 pyramidal neurons in *Syngap1*^{+/-} mice

(A) A coronal section through the mouse brain illustrating where in the mPFC targeted whole-cell recordings were performed. Cg1: cingulated cortex area 1; PL: prelimbic cortex; IL: infralimbic cortex.

(B) A high magnification DIC image of example layer 2/3 neurons and simplified diagram of layer 2/3 circuitry

(C) Example recordings of mEPSC events in PND14 *Syngap1*^{+/-} animals. Scale bar, 20 pA, 100ms.

- (D)** Bar graph and cumulative percentage plots show normal mEPSC amplitude in PND14 *Syngap1*^{+/-} animals (n=15 neurons +/+, n=14 neurons +/-; t(27)=0.40, p=0.69. Two sample K-S test on cumulative percentage distribution Z=1.17, p=0.13)
- (E)** Bar graph and cumulative percentage plots show normal mEPSC frequency in PND14 *Syngap1*^{+/-} animals (n=15 neurons +/+, n=14 neurons +/-; t(27)=1.52, p=0.14 Two sample K-S test on cumulative percentage distribution Z=1.14, p=0.15.)
- (F)** Example recordings of mEPSC events in >9 wks old *Syngap1*^{+/-} animals. Scale bar, 20 pA, 100ms.
- (G)** Bar graph and cumulative percentage plots show increased mEPSC amplitude in >9 wks old *Syngap1*^{+/-} animals (n=12 neurons +/+, n=11 neurons +/-; t(21)=3.61, p=0.0016. Two sample K-S test on cumulative percentage distribution Z=4.34, p<0.001)
- (H)** Bar graph and cumulative percentage plots show increased mEPSC frequency in >9 wks old *Syngap1*^{+/-} animals (n=12 neurons +/+, n=11 neurons +/-; t(21)=3.02, p=0.0065. Two sample K-S test on cumulative percentage distribution Z=3.99, p<0.001)
- (I)** Example recordings of mEPSC events in >9 wks old *Syngap1*^{+/-lx-st} animals. Scale bar, 20 pA, 100ms.
- (J)** Bar graph and cumulative percentage plots show increased mEPSC amplitude in >9 wks old +/lx-st animals (n=9 neurons +/+, n=14 neurons +/-; t(21)=2.57, p=0.018. Two sample K-S test on cumulative percentage distribution Z= 5.42, p<0.001)
- (K)** Bar graph and cumulative percentage plots show slightly increased mEPSC frequency in >9 wks old +/lx-st animals (n=9 neurons +/+, n=14 neurons +/-; t(21)=1.50, p=0.15. Two sample K-S test on cumulative percentage distribution Z= 3.53, p<0.001)
- (L)** Bar graphs and example recordings show reduced mIPSC amplitude and normal mIPSC frequency in in >9 wks old *Syngap1*^{+/-} animals. (n=12 neurons +/+, n=12 neurons +/-; t(22)=2.57, p=0.02 for mIPSC amplitude; t(22)=0.88, p=0.39 for mIPSC frequency). Scale bar, 30 pA, 100ms.
- (M)** Bar graphs and example recordings show normal mIPSC amplitude and normal mIPSC frequency in >9 wks old *Syngap1*^{+/-lx-st} animals. (n=9 neurons +/+, n=7 neurons +/-; t(14)=0.48, p=0.64 for mIPSC amplitude; t(15)=0.40, p=0.70 for mIPSC frequency). Scale bar, 20 pA, 100ms.
- Wild-type(+/+), blue; mutants(+/-), red for all bar graphs. Error bars denote +SEM.
*p<0.05, **p<0.01.

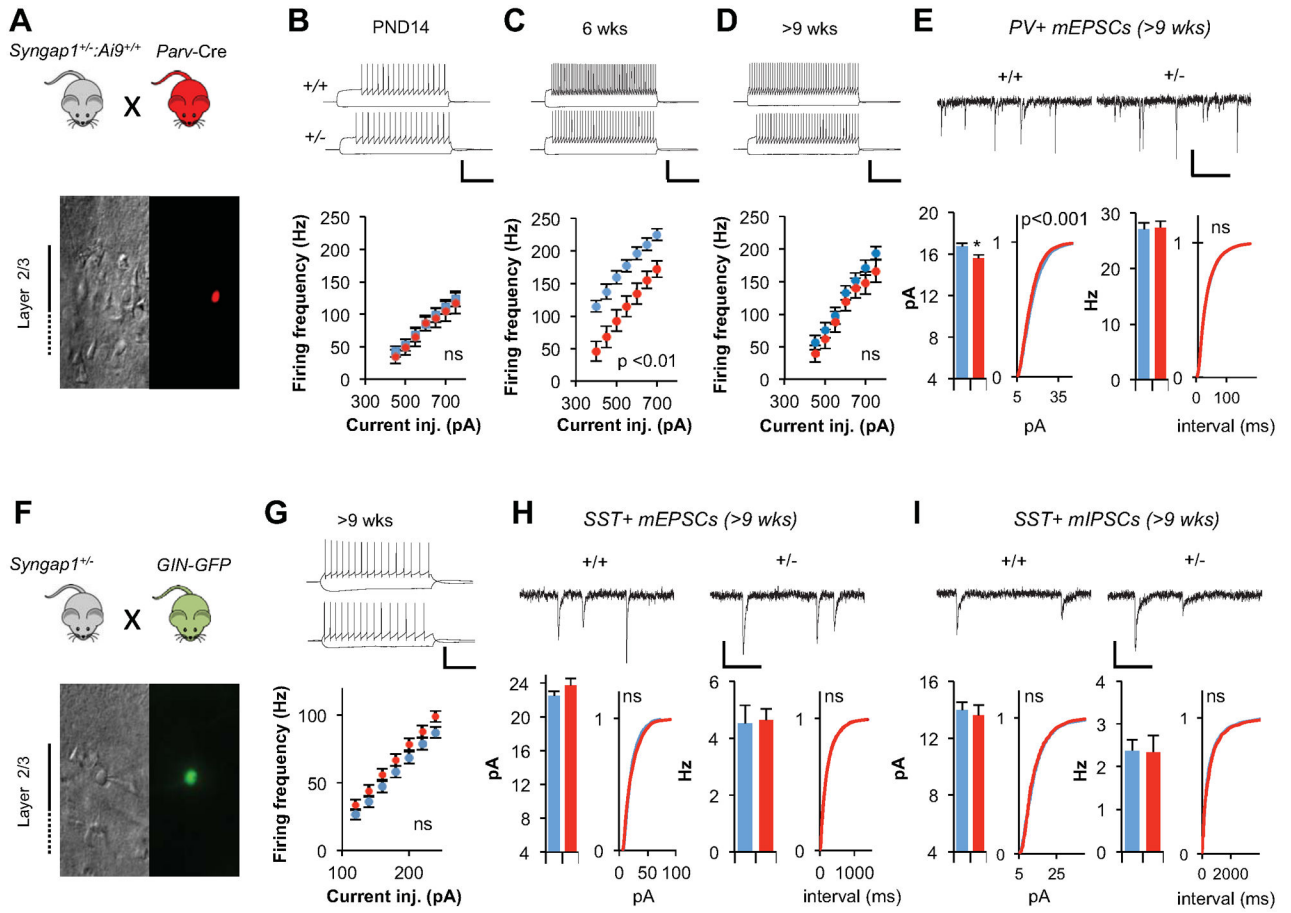


Figure 3. Intrinsic and synaptic properties of Layer 2/3 inhibitory neurons in *Syngap1*^{+/-} mice
(A) Experimental strategy to record from parvalbumin positive (PV+) interneurons in layer2/3. Pictures show DIC and fluorescent image of a parvalbumin positive interneuron.
(B) Normal current injection frequency response curve of PV+ interneurons at PND14. Example traces show firing responses of +/+ and +/- neurons in response to 450 pA, 1 s long current injection (n=11 neurons +/+, n=11 neurons +/-, repeated measures ANOVA genotype effect F(1,20)=0.11, p=0.75, genotype*stimulus level F(6,120)=0.11, p=0.99). Scale bar, 50 mV, 300 ms.
(C) Reduced current injection frequency response curve of PV+ interneurons at 6 weeks. Example traces show firing responses of +/+ and +/- neurons in response to 450 pA, 1 s long current injection (n= 15 neurons +/+, n=16 neurons +/-, repeated measures ANOVA genotype effect F(1,29)=14.74, p=0.001 genotype*stimulus level F(6,174)=1.67, p=0.13). Scale bar, 50 mV, 300 ms.
(D) Normal current injection frequency response curve of PV+ interneurons at >9 weeks. Example traces show firing responses of +/+ and +/- neurons in response to 450 pA, 1 s long current injection (n=18 neurons +/+, n=18 neurons +/-, repeated measures ANOVA genotype effect F(1,34)=0.87, p=0.36, genotype*stimulus level F(6,204)=0.864, p=0.52). Scale bar, 50 mV, 300 ms.
(E) Reduced excitatory input into PV+ interneurons. (Top) Example recordings of mEPSC events in PV+ interneurons. (Left) Bar graph and cumulative percentage plots show reduced

mEPSC amplitude in PV+ interneurons (n=31 neurons +/+, n=34 neurons +/-; t(63)=2.63, p=0.01; Two sample K-S test on cumulative percentage distribution Z=2.15, p=0.0002). (Right) Bar graph and cumulative percentage plots show normal mEPSC frequency in PV+ interneurons (n=31 neurons +/+, n=34 neurons +/-; t(63)=0.14, p=0.88; Two sample K-S test on cumulative percentage distribution; Z=0.58, p=0.89). Scale bar, 15 pA, 125 ms.

(F) Experimental strategy to record from somatostatin positive (SST+) interneurons in layer 2/3. Pictures show DIC and fluorescent image of a somatostatin positive interneuron.

(G) Normal current injection frequency response curve of SST+ interneurons at >9 weeks. Example traces show firing responses of +/+ and +/- neurons in response to 120 pA, 1 s long current injection (n=23 neurons +/+, n=21 neurons +/-, repeated measures ANOVA genotype effect F(1,42)=1.77, p=0.19, genotype*stimulus level F(6,252)=1.02, p=0.41). Scale bar, 50 mV, 300 ms.

(H) Normal excitatory input into SST+ interneurons. (Top) Example recordings of mEPSC events in SST+ interneurons. (Left) Bar graph and cumulative percentage plots show normal mEPSC amplitude in SST+ interneurons (n=12 neurons +/+, n=15 neurons +/-; t(25)=1.19, p=0.24. Two sample K-S test on cumulative percentage distribution Z=1.25, p=0.087) (Right) Bar graph and cumulative percentage plots show normal mEPSC frequency in SST+ interneurons (n=12 neurons +/+, n=15 neurons +/-; t(25)=0.15, p=0.88. Two sample K-S test on cumulative percentage distribution Z=0.77, p=0.59. Scale bar, 15 pA, 125 ms.

(I) Normal inhibitory input into SST+ interneurons. (Top) Example recordings of mIPSC events in SST+ interneurons. (Left) Bar graph and cumulative percentage plots show normal mIPSC amplitude in SST+ interneurons (n=34 neurons +/+, n=22 neurons +/-; t(54)=0.38, p=0.71. Two sample K-S test on cumulative percentage distribution Z=1.15, p=0.14) (Right) Bar graph and cumulative percentage plots show normal mIPSC frequency in SST+ interneurons (n=34 neurons +/+, n=22 neurons +/-; t(54)=0.15, p=0.88. Two sample K-S test on cumulative percentage distribution Z=1.26, p=0.084. Scale bar, 15 pA, 125 ms. Wild-type(+/+), blue; mutants(+/-), red for all bar graphs. Error bars denote +SEM. *p<0.05.

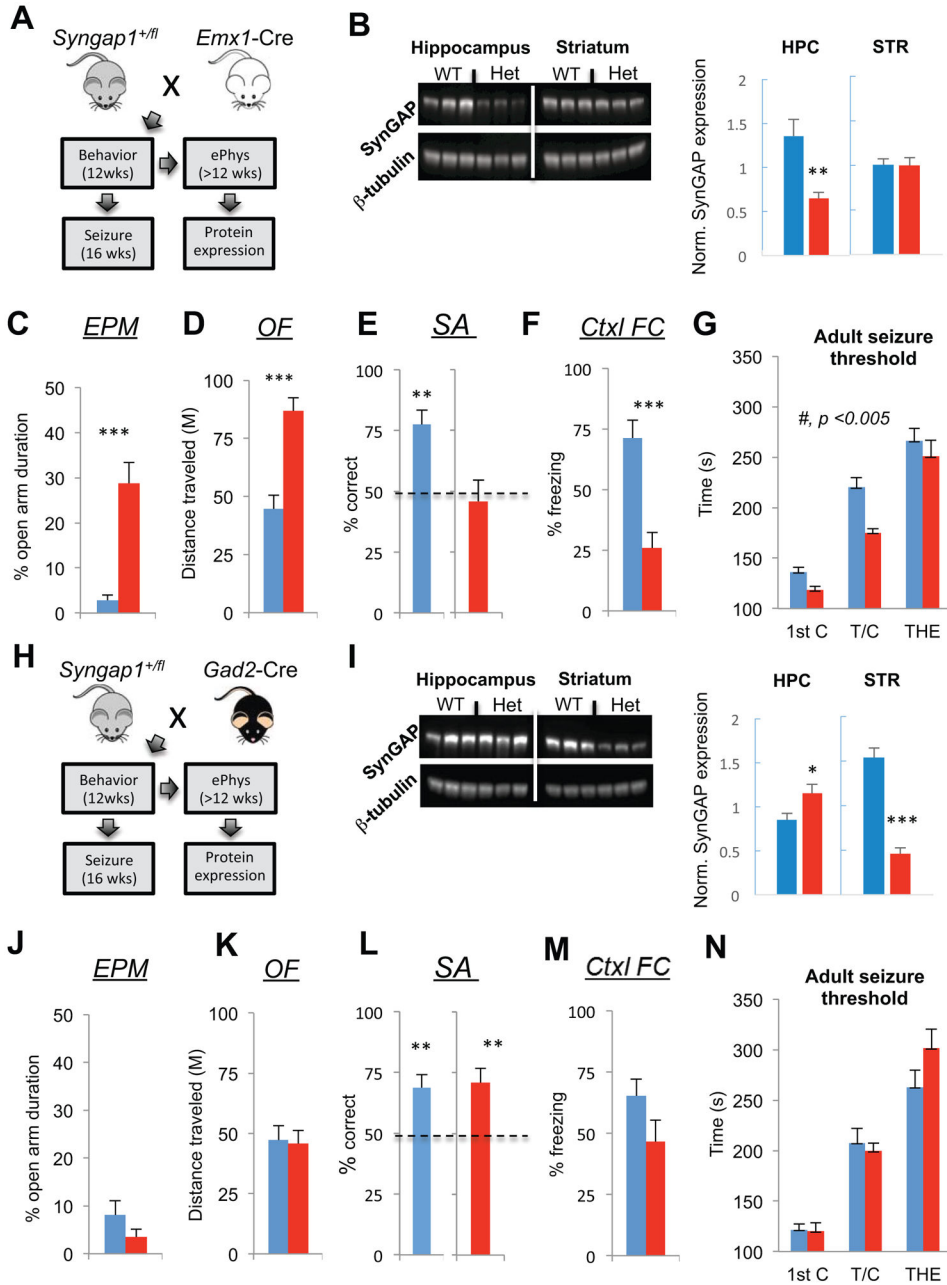


Figure 4. *Syngap1* haploinsufficiency in glutamatergic, but not GABAergic neurons, mimics the germline mutant endophenotype

(A) Experimental schematic depicts mouse breeding strategy and implementation timing of a behavioral test battery and flurothyl-induced seizures for adult offspring of an *Emx1-Cre* x *Syngap1^{+fl}* cross.

(B) Hippocampal (HPC) and dorsal striatal (STR) tissue were dissected from *Emx1-Cre*: *Syngap1^{+/+}* and *Emx1-Cre*: *Syngap1^{+fl}* mice and processed for western blot analysis of SynGAP protein levels normalized to β -tubulin after behavioral and seizure paradigm testing. Normalized density - unpaired t test - n=6 wt, n=6 mutant, HPC: $t(10)=3.45$; p=.0063; STR: $t(10)=0.051$; p=.96.

(C-F) *Emx1*-Cre;Syngap1^{+/+} and *Emx1*-Cre;Syngap1^{+fl} mice were run in a behavioral battery consisting of an elevated plus maze task (EPM), an open field test (OFT), an unforced discrete-two-trial spontaneous alternation task (SA), and a contextual fear conditioning paradigm. Unpaired t tests were performed for EPM, OF, and Ctxl FC tests. One-sample t test with 50% chance level as hypothetical mean were performed with each group for SA. EPM - % Open arm duration: n=16 wt, n=18 mutant, t(32)=5.44, p=5.48E-06. OF - distance traveled (M): n=12 wt, n=12, t(22)=5.18; p=3.39E-05. SA - % alternation: n=10 wt, t(9)=4.71; p=0.0011; n=12 mutant: t(11)=.48; p=.64. Ctxl FC - % freezing: n=7 wt, n=10 mutant, t(15)=4.44, p=.00036

(G) *Emx1*-Cre: Syngap1^{+/+} and *Emx1*-Cre: Syngap1^{+fl} mice were subjected to a flurothyl-induced seizure paradigm. Time taken to reach three separate events, first clonus (1st C), tonic-clonic (T/C), and total hindlimb extension (THE), during the course of the procedure were measured and WT and HET groups compared within each of the two cohorts. RMANOVA – genotype effect: F(1,32)=10.79; p=.0025; genotype x event interaction: F(2,64)=1.67; p=.20.

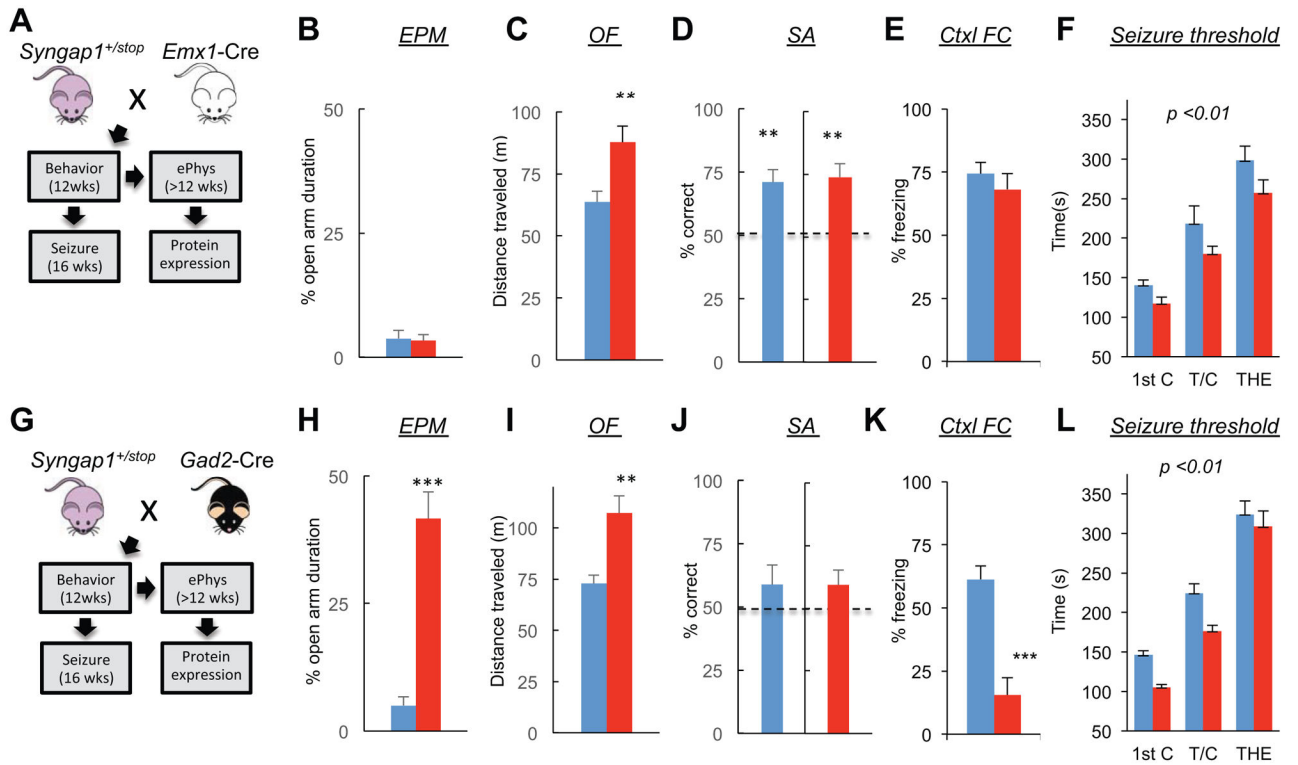
(H) Experimental schematic depicts mouse breeding strategy and implementation timing of a behavioral test battery and flurothyl-induced seizures for adult offspring of a *Gad2*-Cre x Syngap1^{+fl} cross.

(I) Hippocampal (HPC) and dorsal striatal (STR) tissue were dissected from *Gad2*-Cre: Syngap1^{+/+} and *Gad2*-Cre: Syngap1^{+fl} mice and processed for western blot analysis of SynGAP protein levels normalized to β -tubulin after behavioral and seizure paradigm testing. Normalized density - unpaired t test – n=6 wt, n=6 mutant, HPC: t(10)=2.35; p=.040; STR: t(10)=8.61; p=6.12E-06.

(J-M) *Gad2*-Cre: Syngap1^{+/+} and *Gad2*-Cre: Syngap1^{+fl} mice were run in a behavioral battery consisting of an elevated plus maze task (EPM), an open field test (OFT), an unforced discrete-two-trial spontaneous alternation task (SA), and a contextual fear conditioning paradigm. Unpaired t tests were performed for EPM, OF, and Ctxl FC tests. One-sample t test with 50% chance level as hypothetical mean were performed with each group for SA. EPM - % Open arm duration: n=16 wt, n=14 mutant, t(28)=1.30, p=0.20. OF - distance traveled (M): n=12 wt, n=12, t(22)=0.20; p=.85. SA - % alternation: n=12 wt, t(11)=3.45; p=.0055; n=12 mutant, t(11)=3.46; p=.0054. Ctxl FC - % freezing: n=12 wt, n=11 mutant, t(21)=1.71, p=.1027.

(N) *Gad2*-Cre: Syngap1^{+/+} and *Gad2*-Cre: Syngap1^{+fl} mice were subjected to a flurothyl-induced seizure paradigm. Time taken to reach three separate events, first clonus (1st C), tonic-clonic (T/C), and total hindlimb extension (THE), during the course of the procedure were measured and the two groups compared. RMANOVA –genotype effect-F(1,22)=.60; p=.45; genotype x event interaction-F(2,44)=2.42; p=.10.

Wild-type, blue; mutants, red for all bar graphs. Error bars denote +SEM. *p<0.05, **p<0.01, ***p<0.001.



unforced discrete-two-trial spontaneous alternation task (SA), and a contextual fear conditioning paradigm. Unpaired t tests were performed for EPM, OF, and Ctxl FC tests. One-sample t test with 50% chance level as hypothetical mean were performed with each group for SA. EPM - % Open arm duration: n=17 wt, n=16 mutant, $t(31)=6.83$, $p=9.92E-08$. OF - distance traveled (M): n=17 wt, n=16, $t(31)=3.78$; $p=.00067$. SA - % alternation: n=17 wt, $t(16)=1.14$; $p=.27$; n=16 mutant, $t(15)=1.57$; $p=.14$. Ctxl FC - % freezing: n=13 wt, n=12 mutant, $t(23)=5.36$, $p=1.91E-05$.

(L) *Gad2-Cre: Syngap1^{+/+}* and *Gad2-Cre: Syngap1^{+/-x-st}* mice were subjected to a flurothyl-induced seizure paradigm. Time taken to reach three separate events, first clonus (1st C), tonic-clonic (T/C), and total hindlimb extension (THE), during the course of the procedure were measured and the two groups compared. RMANOVA – genotype effect- $F(1,23)=11.69$; $p=.0024$; genotype x event interaction- $F(2,46)=0.96$; $p=0.39$. Wild-type, blue; mutants, red for all bar graphs. Error bars denote +SEM. * $p<0.05$, ** $p<0.01$, *** $p<0.001$.

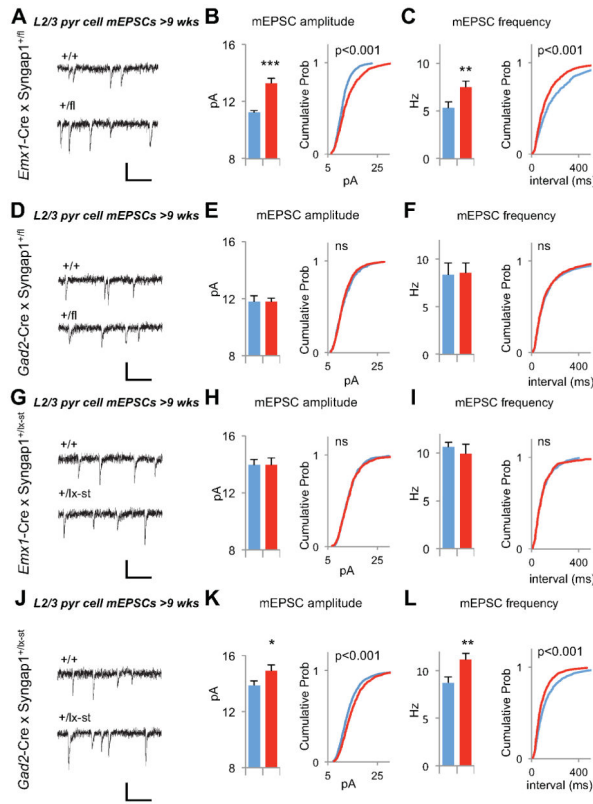


Figure 6. Enhanced Layer 2/3 excitatory synaptic function is an indicator of reduced cognition in *Syngap1* mutants

(A) Example recordings of mEPSC events from +/+ and +/fl mice obtained by *Emx1-Cre* x *Syngap1*^{+/-} cross. Scale bar, 20 pA, 100ms.

(B) Bar graph and cumulative percentage plots show increased mEPSC amplitude in *Emx1-Cre*;/+fl mice (n=10 +/+, n=12 +/fl, t(20)=4.92, p=8.2×10⁻⁵. Two sample KS test on cumulative percentage distribution Z=4.24, p<0.001)

(C) Bar graph and cumulative percentage plots show increased mEPSC frequency in *Emx1-Cre*;/+fl mice (n=10 +/+, n=12 +/fl, t(20)=2.26, p=0.035. Two sample K-S test on cumulative percentage distribution Z=3.39, p<0.001)

(D) Example recordings of mEPSC events from +/+ and +/fl mice obtained by *Gad2-Cre* x *Syngap1*^{+/-} cross. Scale bar, 20 pA, 100ms.

(E) Bar graph and cumulative percentage plots show normal mEPSC amplitude in *Gad2-Cre*;/+fl mice (n=11 +/+, n=11 +/fl, t(20)=0.03, p=0.98. Two sample K-S test on cumulative percentage distribution Z=1.12, p=0.16)

(F) Bar graph and cumulative percentage plots show normal mEPSC frequency in in *Gad2-Cre*;/+fl mice (n=11 +/+, n=11 +/fl, t(20)=0.14, p=0.89. Two sample K-S test on cumulative percentage distribution Z=0.69, p=0.73)

(G) Example recordings of mEPSC events from +/+ and +/lx-st mice obtained by *Emx1-Cre* x *Syngap1*^{+/-lx-st} cross. Scale bar, 20 pA, 100ms.

(H) Bar graph and cumulative percentage plots show normal mEPSC amplitude in *Emx1-Cre*;/+lx-st mice (n=17 +/+, n=13 +/lx-st, t(28)=0.00045, p=0.99. Two sample K-S test on cumulative percentage distribution Z=0.62, p=0.83)

(I) Bar graph and cumulative percentage plots show normal mEPSC frequency in *Emx1-Cre;+/lx-st* mice (n=17 +/+, n=13 +/lx-st, t(28)=0.68, p=0.50. Two sample K-S test on cumulative percentage distribution Z=0.50, p=0.96)

(J) Example recordings of mEPSC events from +/+ and +/lx-st mice obtained by *Gad2-Cre x Syngap1^{+/lx-st}* cross. Scale bar, 20 pA, 100ms.

(K) Bar graph and cumulative percentage plots show increased mEPSC amplitude in *Gad2-Cre;+/lx-st* mice (n=19 +/+, n=19 +/lx-st, t(36)=2.49, p=0.017. Two sample K-S test on cumulative percentage distribution Z=3.86, p<0.001)

(L) Bar graph and cumulative percentage plots show increased mEPSC frequency in *Gad2-Cre;+/lx-st* mice (n=19 +/+, n=19 +/lx-st, t(36)=3.15, p=0.0033. Two sample K-S test on cumulative percentage distribution Z=4.34, p<0.001)

Wild-type, blue; mutants, red for all bar graphs. Error bars denote +SEM. *p<0.05, **p<0.01, ***p<0.001.

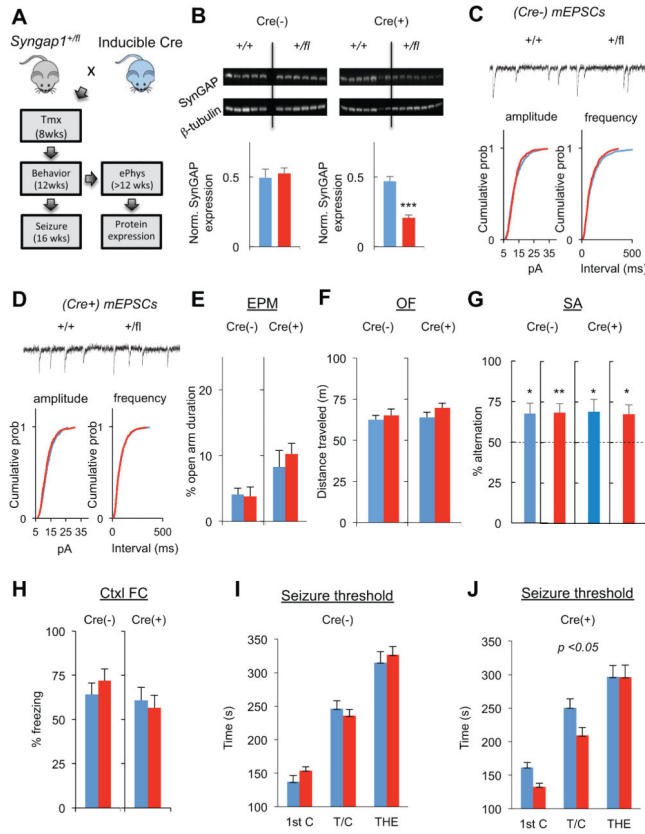


Figure 7. Global induction of *Syngap1* haploinsufficiency in adulthood has a minimal impact on L2/3 synaptic function and behavior

(A) Experimental strategy to induce *Syngap1* haploinsufficiency during adulthood. Following a cross between *Syngap1*^{+/*fl*} and hemizygous CreERT transgenic mice, the following four groups of mice were generated and used for experiments: Cre(-)/*Syngap1*^{+/*+*}, Cre(-)/*Syngap1*^{+/*fl*}, Cre(+)/*Syngap1*^{+/*+*}, Cre(+)/*Syngap1*^{+/*fl*}. All animals were injected with tamoxifen at 8 weeks of age.

(B) Hippocampal (HPC) tissue was dissected from Cre(-)/*Syngap1*^{+/*+*}, Cre(-)/*Syngap1*^{+/*fl*}, Cre(+)/*Syngap1*^{+/*+*}, and Cre(+)/*Syngap1*^{+/*fl*} mice and processed for western blot analysis of SynGAP protein levels normalized to β-tubulin after behavioral and seizure paradigm testing. Normalized density - unpaired t test – Cre(-): n=5 wt, n=6 mutant, t(9)=0.44; p=.66; Cre(+): t(12)=6.86; p=.1.74E-05.

(C) Cumulative percentage plots and example recordings show normal mEPSC amplitude and frequency in (Cre-) animals. (n=11 +/+, n=11 +/fl; mean mEPSC amplitudes 12.59±0.48 +/+, 12.83±0.35 +/fl, t(20)=0.40, p=0.69; mean mEPSC frequencies 10.14±1.07 +/+, 11.25±0.65 +/fl, t(20)=0.89, p=0.38; Two sample KS test on cumulative percentage distributions: Z=1.07, p=0.2 for mEPSC amplitude; Z=1.02, p=0.25 for mEPSC interevent interval)

(D) Cumulative percentage plots and example recordings show normal mEPSC amplitude and frequency in (Cre+) animals. (n=12 +/+, n=12 +/fl; mean mEPSC amplitudes 13.04±0.24 +/+, 12.67±0.47 +/fl; mean mEPSC frequencies 12.33±0.67 +/+, 12.08±0.74 +/fl, t(22)=0.70, p=0.49; t(20)=0.25, p=0.80; Two sample K-S test on cumulative percentage

distributions $Z=1.28$, $p=0.07$ for mEPSC amplitude; $Z=0.59$, $p=0.88$ for mEPSC interevent interval).

(E–H) $Cre(-)/Syngap1^{+/+}$, $Cre(-)/Syngap1^{+/fl}$, $Cre(+)/Syngap1^{+/+}$, $Cre(+)/Syngap1^{+/fl}$ mice were run in a behavioral battery consisting of an elevated plus maze task (EPM), an open field test (OFT), an unforced discrete-two-trial spontaneous alternation task (SA), and a contextual fear conditioning paradigm. Unpaired t tests were performed for EPM, OF, and Ctxl FC tests. One-sample t test with 50% chance level as hypothetical mean were performed with each group for SA. EPM - % Open arm duration – $Cre(-)$: $n=15$ wt, $n=18$ mutant, $t(31)=0.16$, $p=.87$; $Cre(+)$: $n=16$ wt, $n=17$ mutant, $t(31)=0.68$, $p=.50$. OF - distance traveled (M) – $Cre(-)$: $n=15$ wt, $n=16$ mutant, $t(29)=.55$, $p=.59$; $Cre(+)$: $n=16$ wt, $n=17$ mutant, $t(31)=1.40$, $p=.17$. SA - % alternation – $Cre(-)/Syngap1^{+/+}$: $t(12)=2.63$, $p=.022$; $Cre(-)/Syngap1^{+/fl}$: $t(14)=3.21$, $p=.0062$; $Cre(+)/Syngap1^{+/+}$: $t(15)=2.42$, $p=.028$; $Cre(+)/Syngap1^{+/fl}$: $t(12)=2.92$, $p=.013$. Ctxl FC - % freezing: $Cre(-)$: $n=11$ wt, $n=11$ mutant, $t(20)=0.83$, $p=.41$. $Cre(+)$: $n=13$ wt, $n=9$ mutant, $t(20)=0.4$, $p=.69$.

(I–J) $Cre(-)/Syngap1^{+/+}$, $Cre(-)/Syngap1^{+/fl}$, $Cre(+)/Syngap1^{+/+}$, $Cre(+)/Syngap1^{+/fl}$ mice were subjected to a flurothyl-induced seizure paradigm. Time taken to reach three separate events, first clonus (1st C), tonic-clonic (T/C), and total hindlimb extension (THE), during the course of the procedure were measured and WT and HET groups compared within each of the $Cre(-)$ and $Cre(+)$ groups. RMANOVA – $Cre(-)$: genotype effect- $F(1,25)=0.22$; $p=0.64$; genotype x event interaction- $F(2,50)=0.66$; $p=0.52$. $Cre(+)$: genotype effect- $F(1,22)=4.58$; $p=0.044$; genotype x event interaction- $F(2,44)=2.18$; $p=0.12$. Wild-type, blue; mutants, red for all bar graphs. Error bars denote +SEM. * $p<0.05$, ** $p<0.01$, *** $p<0.001$.

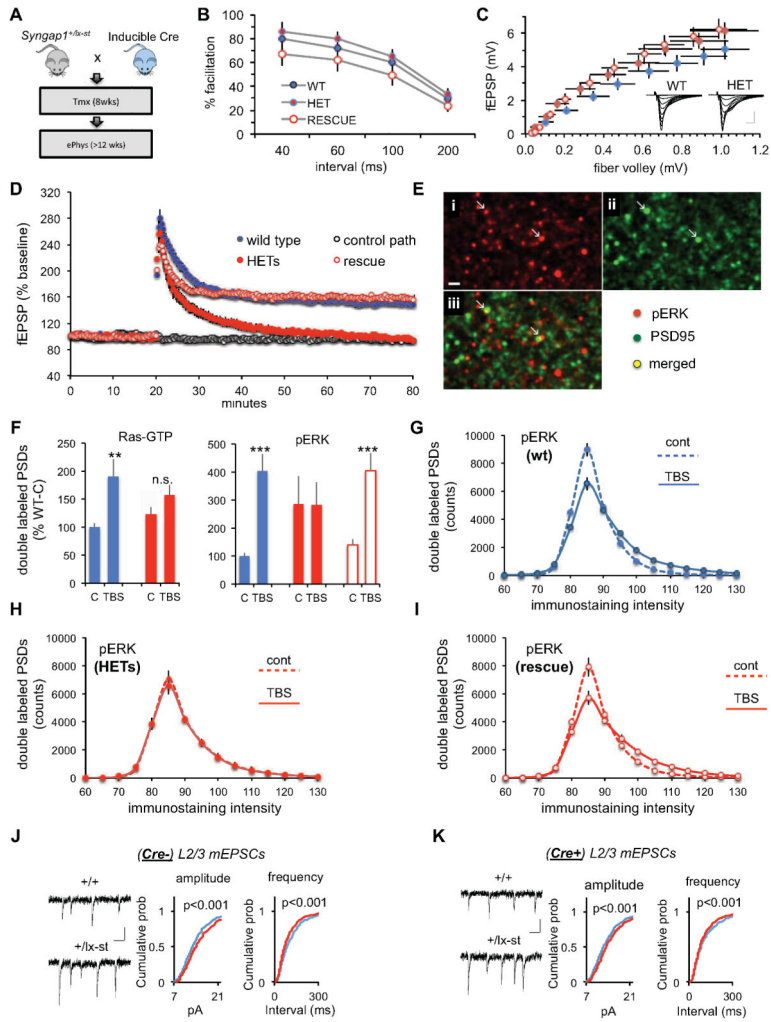


Figure 8. Global rescue of pathogenic *Syngap1* mutations in adulthood has a differential effect on synaptic defects originating in distinct types of EMX1+ neurons

(A) Experimental strategy to induce *Syngap1* haploinsufficiency during adulthood. Following a cross between *Syngap1*^{+fl} and hemizygous CreERT transgenic mice, the following four groups of mice were generated and used for experiments: Cre(-)/*Syngap1*^{+/+}, Cre(-)/*Syngap1*^{+fl}, Cre(+)/*Syngap1*^{+/+}, Cre(+)/*Syngap1*^{+fl}. All animals were injected with tamoxifen at 8 weeks of age.

(B) Paired pulse facilitation curves (initial slope of fEPSP vs. intervals between two stimulation pulses) for the indicated three groups of hippocampal slices. There were no statistically meaningful differences.

(C) Input/output curves (response size vs. magnitude of fiber volley) for the three groups. Stimulation current was increased across a series of steps and the two variables measured. *Inset*: representative traces collected from wild type (WT) and HET mice at each step in the input/output curve. Scale: 1mV/5ms.

(D) Magnitude of long-term potentiation (LTP) following delivery of a single train of five theta bursts. The slope of the fEPSP was normalized to the mean value for a ten minute

baseline period; shown are group means and standard errors. The control path, to the same site at which LTP was recorded, received 3/min pulses throughout the session.

(E) Dual immunostaining (PSD95 and p-ERK1/2) of a section through a hippocampal slice collected 2 minutes after a theta burst train. The images were processed using the fluorescence deconvolution tomography techniques described in Methods. Intensely labeled structures are shown. (i: p-ERK1/2; ii: PSD95; iii: merged images; also note arrows).

(F) Number of PSD95-positive puncta satisfying size and eccentricity constraints for synapses associated with very dense labeling for Ras-GTP (left) or pERK (right) from the zone surrounding a recording electrode in slices that received theta bursts (TBS) or low frequency baseline stimulation only (C). Values are percents of the double labeling counts for wild-type slices given control baseline stimulation. Asterisks denote statistical significance for the matched control vs. TBS cases (2-tailed t-tests for unequal variance. ** $p=0.012$; *** $p=0.002$; **** $p<0.0001$).

(G) Counts of synapses associated with the indicated intensities of pERK1/2 labeling for slices given control baseline stimulation (dashed line) or TBS (solid line) from wild-type slices; interaction term for two 2-way ANOVA comparing curves for control vs. TBS groups ($F(31,928)=14.54$; $p<0.0001$).

(H) Same as panel F for control and TBS cases from 'rescue' slices ($F(31,416)=7.44$; $p<0.0001$).

(I) Same as panel F for slices prepared from heterozygotes ($F(31,416)=0.33$; $p>0.95$).

(J) Cumulative percentage plots and example recordings show increased mEPSC amplitude and frequency in (Cre⁻) animals. ($n=17$ +/+, $n=17$ +/lx-st; mean mEPSC amplitudes 14.09 ± 0.30 +/+, 15.16 ± 0.41 +/lx-st, $t(32)=2.08$, $p=0.045$; mean mEPSC frequencies 8.89 ± 0.60 +/+, 11.11 ± 0.75 +/lx-st, $t(32)=2.30$, $p=0.028$; Two sample K-S test on cumulative percentage distributions: $Z=2.89$, $p<0.001$ for mEPSC amplitude; $Z=3.22$, $p<0.001$ for mEPSC interevent interval)

(K) Cumulative percentage plots and example recordings show increased mEPSC amplitude and frequency in (Cre⁺) animals. ($n=21$ +/+, $n=16$ +/lx-st; mean mEPSC amplitudes 13.79 ± 0.29 +/+, 14.79 ± 0.30 +/lx-st, $t(35)=2.31$, $p=0.027$; mean mEPSC frequencies 9.16 ± 0.66 +/+, 10.95 ± 0.75 +/lx-st, $t(35)=2.03$, $p=0.05$; Two sample K-S test on cumulative percentage distributions $Z=2.92$, $p<0.001$ for mEPSC amplitude; $Z=2.80$, $p<0.001$ for mEPSC interevent interval).